HYBRID BROADBAND GROUND-MOTION SIMULATIONS FOR THE 2016 AMATRICE EARTHQUAKE, CENTRAL ITALY, AND SENSITIVITY OF GROUND-MOTION TO EARTHQUAKE SOURCE PARAMETERS

36th General Assembly of the European Seismological Commission
2-7 September 2018 | Valletta - Malta

M. Pischiutta, A. Akinci, E. Tinti, A. Cirella, A. Herrero

INGV - Istituto Nazionale di Geofisica e Vulcanologia, Rome (Italy)

Abstract

On 24th August 2016 at 01:36 UTC a M_w 6.0 earthquake struck several villages in central Italy, among which Accumoli, Amatrice and Arquata del Tronto. It caused 299 fatalities, major destruction and extensive damage in the surrounding area (up to 11 intensity degree). The earthquake was recorded by 350 digital accelerometers belonging to the National Accelerometric Network (RAN) of the Italian Department of Civil Protection, to the National Seismic Network (Rete Sismica Nazionale, RSN) of the Istituto Nazionale di Geofisica e Vulcanologia (INGV), and to other local networks. This earthquake ruptured a NW–SE oriented normal fault, according the prevailing extensional tectonics of the area. The maximum acceleration was observed at Amatrice station (AMT) with epicentral distance of 15 km, reaching 916 cm/s^2 and 445.6 cm/s^2 on E-W and N-S components, respectively. Motivated by the high levels of observed ground motion and damage, we have computed synthetics broadband time series for engineering purposes.
To produce high-frequency seismograms, we have used a stochastic finite-fault model approach based on dynamic corner-frequency.

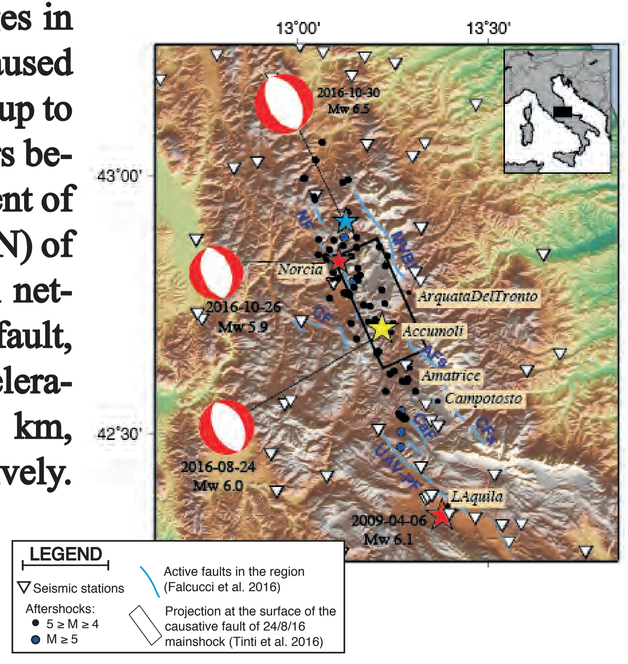

Figure 1
Map showing the regional setting of the August 24, 2016 central Italy mainshock. The epicenter of 24 August M_w 6.0 mainshock is indicated with a yellow star. We also show epicenters of October 26, M_w 5.9 (red star), October 30, M_w 6.5 (cyan star) and April 6 2009, M_w 6.1 earthquakes.

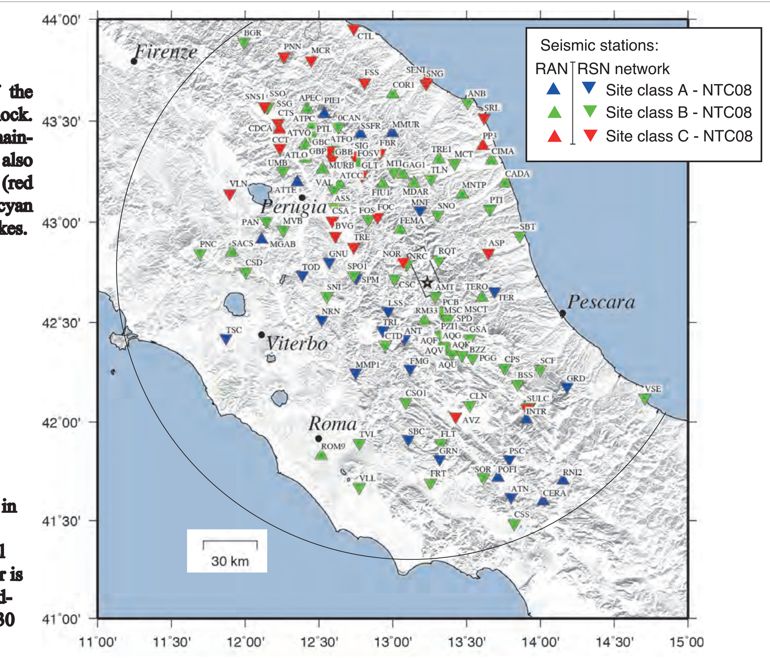

Figure 2
Map showing stations considered in this study, belonging to RAN and RSN networks, up to an epicentral distance of 150 km. Symbol color is related to site classification according to NTC-08 on the basis of Vs30 parameter.

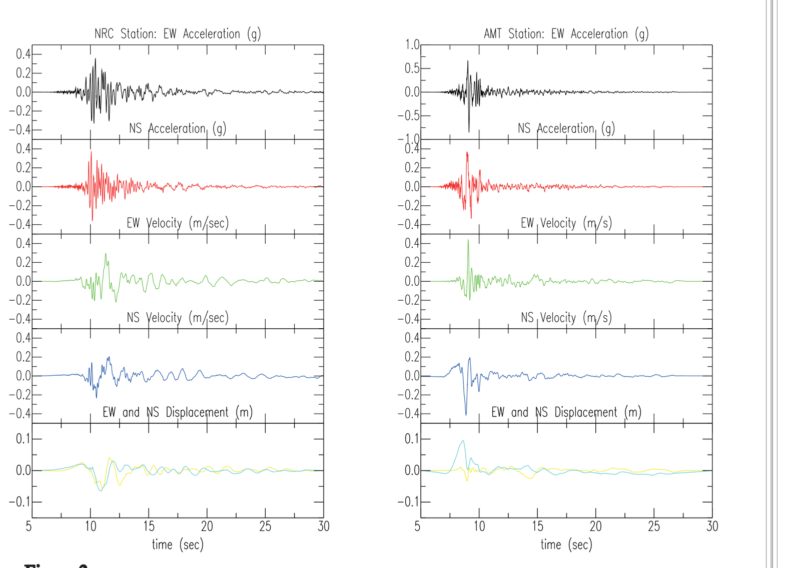

Figure 3
Recorded signals (acceleration, velocity and displacement) at near fault stations NRC (Norcia) and AMT (Amatrice).

Method

- Low-frequency seismograms were obtained by Tinti et al.(2016) inverting the recordings of the 26 three-component digital accelerometers of the RAN and INGV networks closest to the epicenter (Depi< ~45km). The inversion code is based on the method of Hartzell & Heaton (1983), as implemented by Dreger et al. (2005) and consists of a nonnegative, least squares inversion method with simultaneous smoothing and damping. This approach assumes a constant rupture velocity and allows us to use multiple time windows to account for potential variations in rupture speed and local rise time. The Green's functions were obtained using the CIA (Central Italian Apennines) velocity model (Herrmann et al., 2011). The fault plane attitude is 156° strike and 50° dip, as inferred from the TDMT solution. In this study we adopted an update version of Tinti et al. (2016) solution to account for the correction of data at station AMT (released after the publication of the paper).
- We integrated the dynamically simulated earthquake scenarios adding an additional complexity with a k^2like-slip distribution, based on a fractal sum of asperities following Ruiz et al. (2011) and Herrero and Bernard (1994). To link the HF part to the large wavelength slip model, it was used as a probability density function to draw the asperities on the fault.
- We produced high-frequency seismograms using a stochastic finite-fault model approach based on dynamic corner frequency (Motazedian & Atkinson,2005).
- Broadband synthetic time series were obtained by merging high frequency and low frequency seismograms.

Source Parameters	Tinti et al. (2016)	Cirella & Piatanesi (2016)
Fault orientation (strike & dip)	156°-50°	156°-50°
Fault dimensions (km)	26.5 x 15	30 x 17.5
Moment magnitude	6.0	6.0
Corner of the upper edge (lat,lon)	42.87726 13.21006	42.8921 13.21078
Depth of the top of the fault plane (km)	0.25	0,25
Subfault dimensions (km)	0.16 x 0.16	2.5 x 2.5
Source spectrum model	Single corner-frequency ω2	Single corner-frequency ω2
Stress parameter Δσ (bars)	120,00	120,00
Shear-wave velocity at source depth β (km/s)	3.2	3.2
Density at source depth ρ (gm/cc)	2.8	2.8
Rupture propagation speed (km/s)	fixed at 3.1 km/s	variable following Cirella & Piatanesi (2016)
Pulsing area percentage	0.5	0.5

Table 1
Spectral source parameters used in the High Frequency (HF) Stochastic Ground-Motion Simulations used for Tinti et al. (2016) slip model and Cirella & Piatanesi (2016) slip and velocity model.

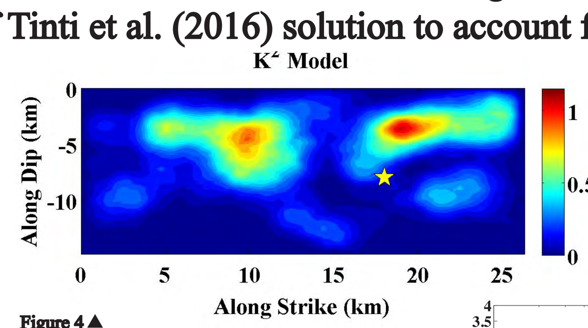

Figure 4
Slip model distribution by Tinti et al. (2016) adopted in this study adding an additional complexity of k^2 like-slip distribution. The yellow star indicates the hypocentre of the 24 August 2016 mainshock.

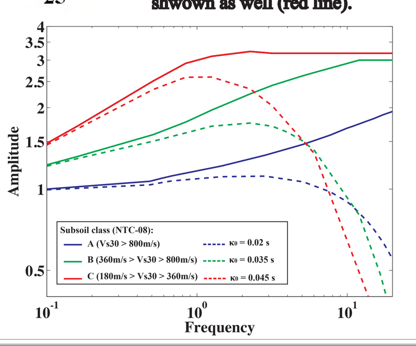

Figure 5
Site amplification curves (solid lines) adopted in this study and generated for sites representative of classes A, B and C following the Italian seismic design (NTC-08). The effect of attenuation is added considering the coefficient k_0 (dotted lines).

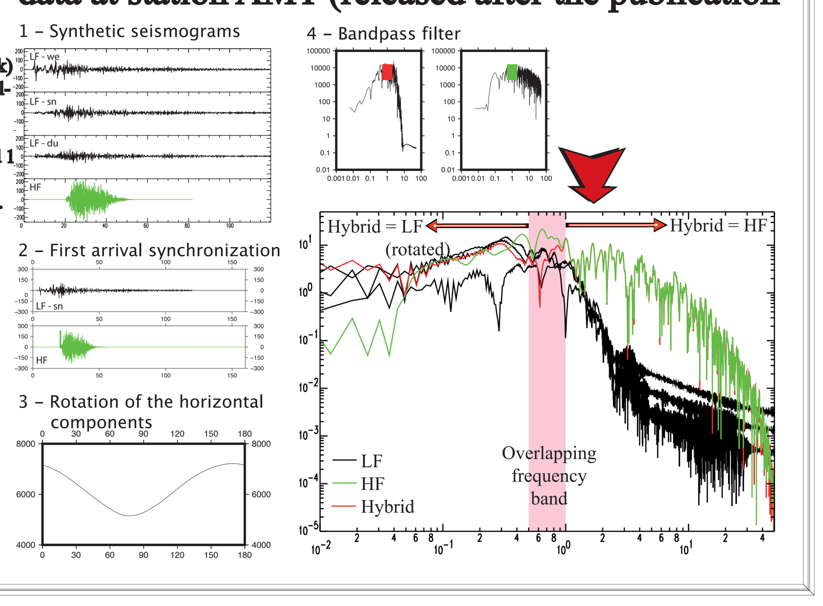

Figure 6
Example of low-frequency (LF - black) and high-frequency (HF - green) acceleration synthetics (left top panels). Both spectra are combined using a complementary filter between 0.5 and 1 Hz after time synchronization and rotation of the horizontal components. The resulting acceleration Fourier is shwown as well (red line).

Results

1. Simulated signals

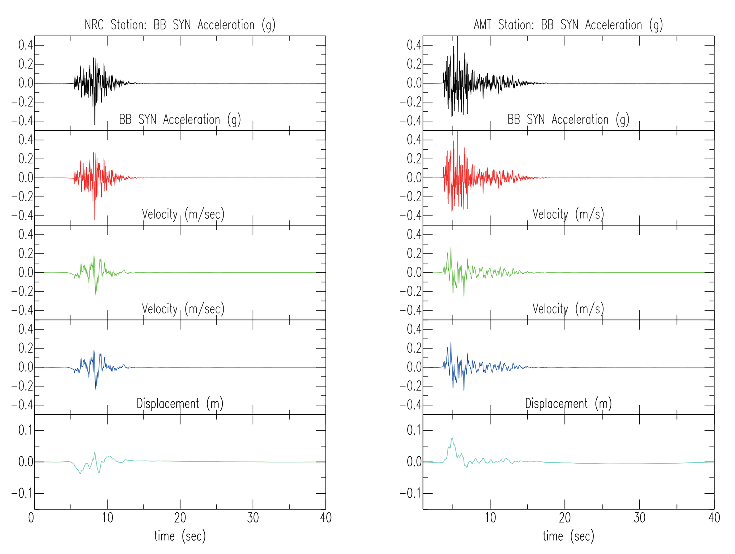

Figure 7
Hybrid simulated time histories (acceleration, velocity and displacement) at near-fault stations NRC (Norcia) and AMT (Amatrice) obtained using Tinti et al. (2016) slip model.

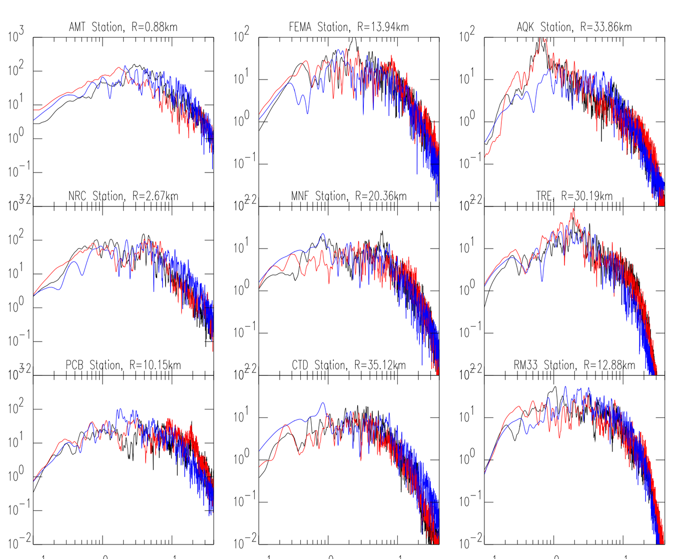

Figure 8
Hybrid Fourier spectra (blue) at selected stations NRC (Norcia) and AMT (Amatrice) obtained using Tinti et al. (2016) slip model. Recorded data are reported as well (NS - component, red - EW component).

2. Comparison with GMPEs

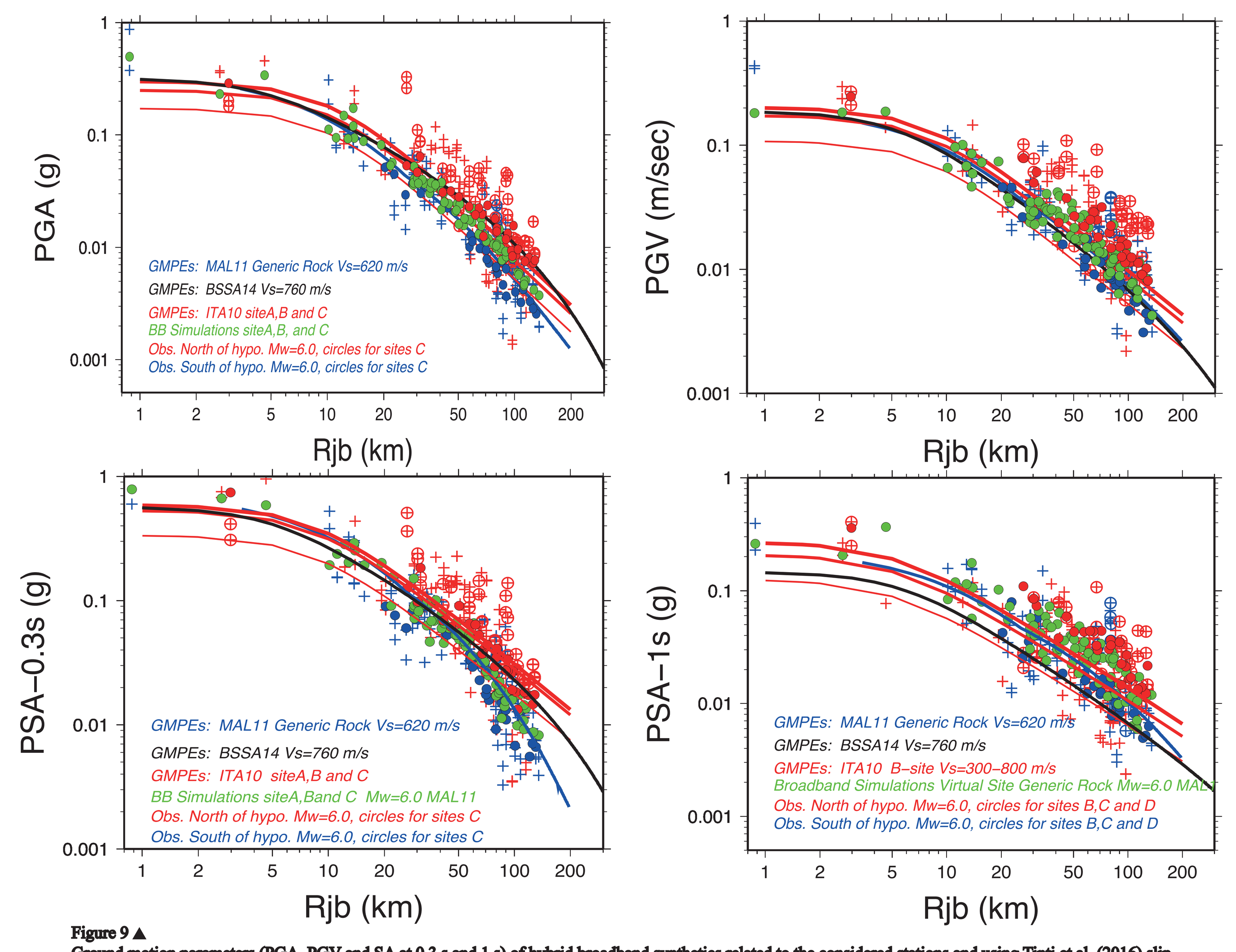

Figure 9
Ground motion parameters (PGA, PGV and SA at 0.3 s and 1 s) of hybrid broadband synthetics related to the considered stations and using Tinti et al. (2016) slip model. Symbol color is related to the seismic site class according to NTC-08. Comparison with the following ground-motion predictive equations (GMPEs): (1) GMPEs developed within context of the Next Generation Attenuation (NGA) models project, Boore et al. (2014; hereafter, BA2014); (2) Italian model of Bindi et al. (2010; herafter, ITA2010), Malagnini et al. (2011; hereafter MAL11). The recorded values on the two horizontal components at the seismic stations are reported as well (crosses - A,B sites; circle+cross - C sites).

3. Residuals

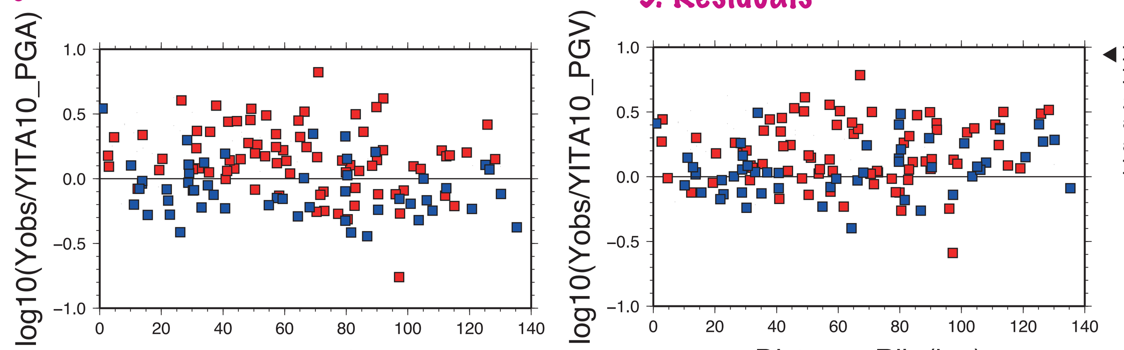

Figure 10
Residuals between observed ground motion parameters (PGAs and PGVs) and the expected ones according to GMPEs (blue - BSSA14; red - ITA10).

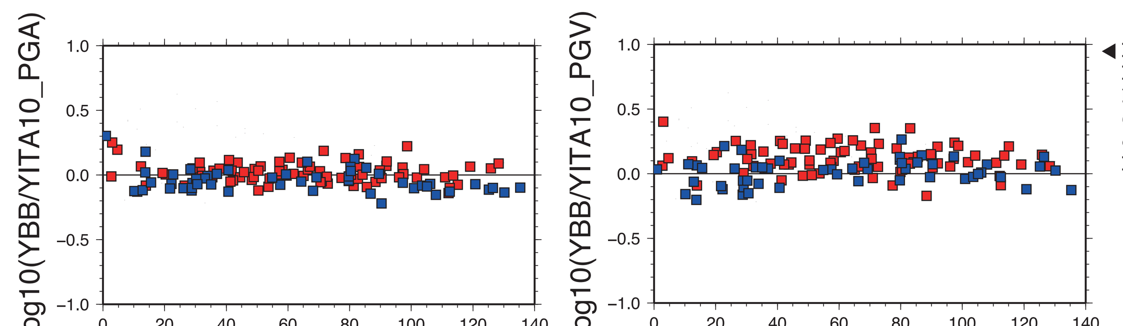

Figure 11
Residuals between values of simulated ground motion parameters (PGAs and PGVs) and the expected ones according to GMPEs (blue - BSSA14; red - ITA10).

- Synthetic hybrid waveforms and Fourier amplitude are generally compatible with records. At near fault stations (AMT and NRC) synthetic seismic signals well reproduce the source velocity pulse.
- At all distances ground motion parameters better agree with ITA10 GMPE than with BSSA14. In the near field, both the observed and simulated PGAs and PGVs are underestimated by GMPEs due to the source complexity. Residuals are generally higher for B and C sites suggesting that GMPEs underestimate modelled ground motion due to site amplification.
- We observe that the largest ground shaking is obtained along the rupture fault plane, PGVs distribution shows that the strongest ground shaking is observed within the surface projection of the fault around the location of the two large-slip asperities.
- While the near-field results are governed by the source effects, intermediate distances are controlled by the path effects, ground motion levels becoming comparable at similar distances.

4. Spatial distribution of ground motion parameters

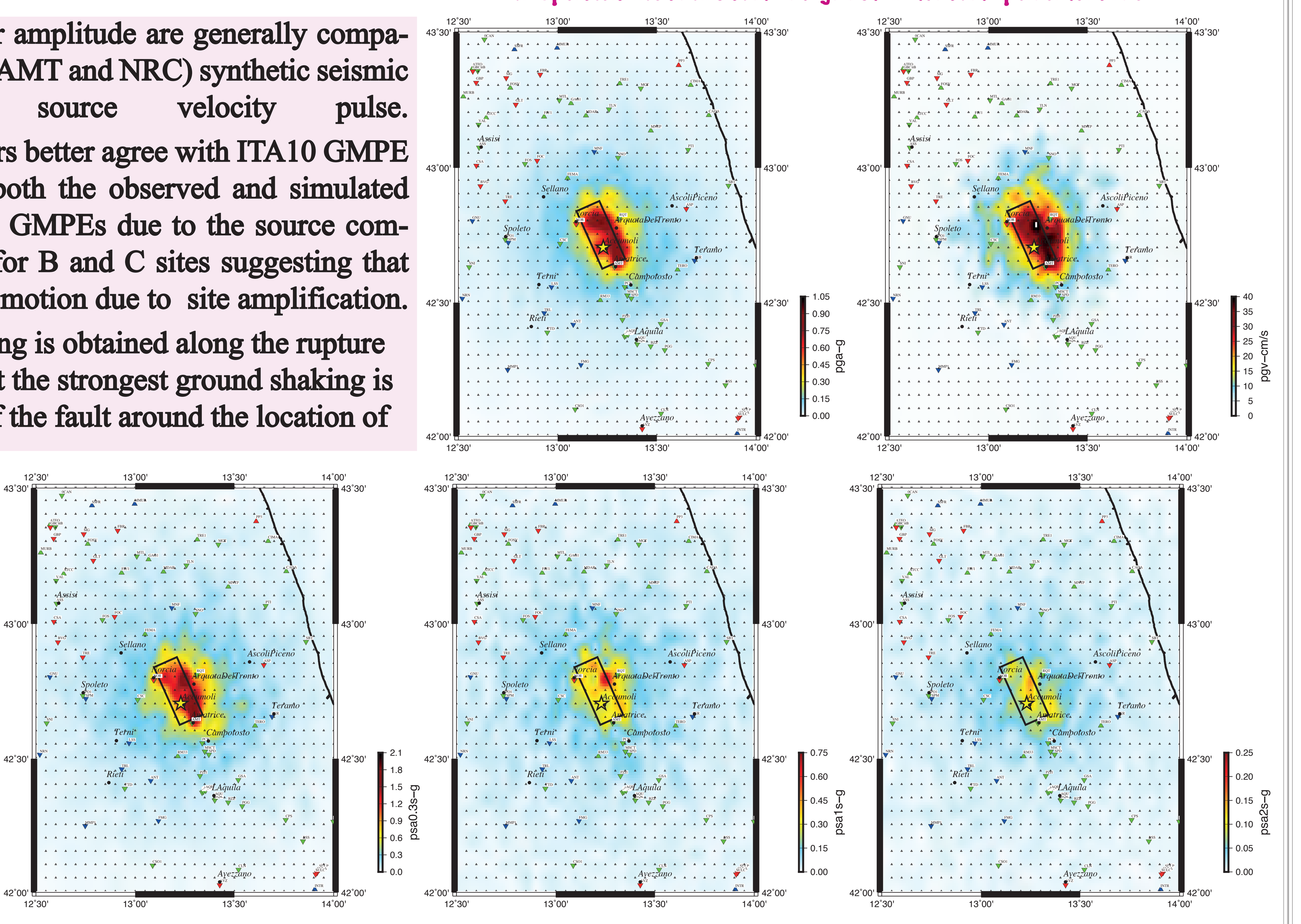

Figure 12
Spatial distributions of broadband ground motion (hybrid horizontal component) at 961 virtual stations located following a regular grid spacing of 0.5 km x 0.5 km, in terms of peak ground acceleration (PGA, g), peak ground velocity (PGV, cm/s) and pseudospectral acceleration at 0.3, 1 and 2s. Simulations were performed using the parameters given in Table 1.

5. Directivity and site effects

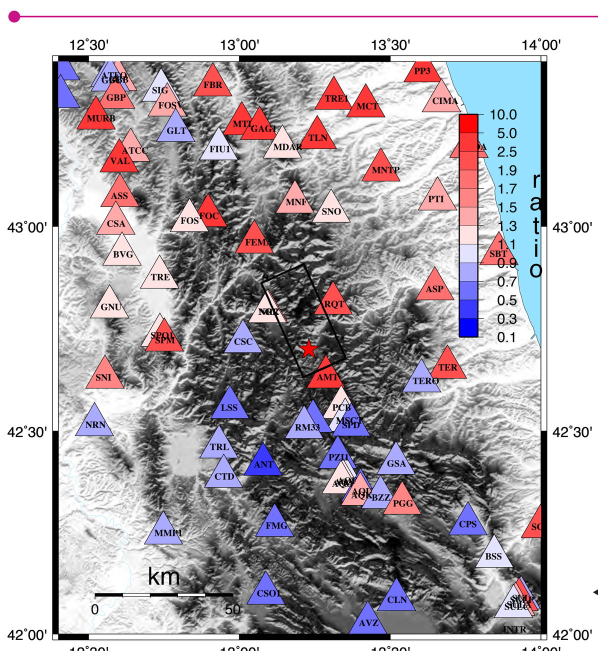

Following Pischiutta et al. (2016) approach, who have found higher ground motion levels towards NE and lower levels in the NW and SW sectors (see Fig. 13), we have plotted the residuals between simulated PGAs and PGVs and the ones calculated using GMPEs using a map view. The areal distribution of PGA residuals (Fig.14) suggests an evident forward directivity effect caused by the fast rupture propagation towards NW direction along the seismogenic fault, according to other authors (Lanzano et al., 2016; Calderoni et al., 2016; Ren et al. 2017). This tendency is also evidenced by the acceleration spectra at stations in the forward and backward directivity sectors (Fig.15).

Figure 13
Areal distribution of PGA ratio, calculated between obsetved and predicted values on the basis of ITA10 GMPE (PGAOBS/PGAITA10) at the considered stations of RAN and RSN networks, following Pischiutta et al. (2016).

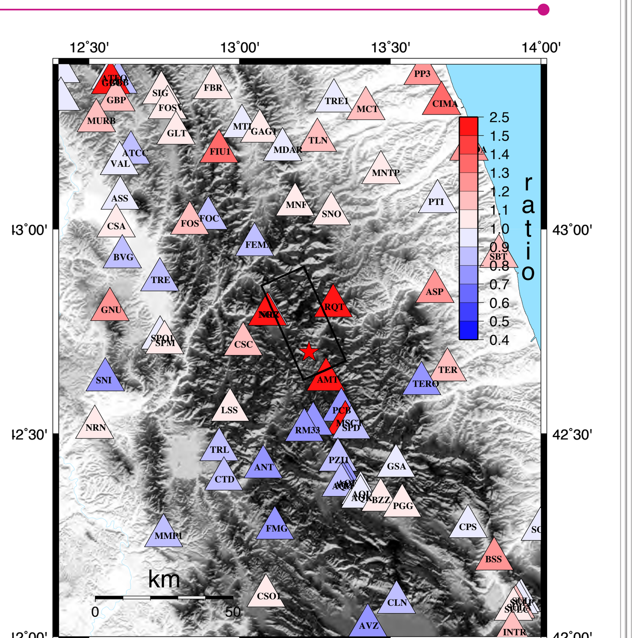

Figure 14
Areal distribution of PGA ratio, between simulated values and predicted ones on the basis of ITA10 GMPE (PGASIMPGAITA10) at the considered stations of RAN and RSN networks.

The Vs30-based soil site classification adopted in seismic code has some limitations leading in many cases to not take into account site-specific amplification effects. An example is represented by stations AQV, AQF and AQK, located about the same distance, all in the B-class. The PGVs simulations strongly underestimate observation. This is due to local site amplification effects produced by a well-known impedance contrast occurring at depth larger than 30 m in a sedimentary basin (e.g. De Luca et al, 1996; Akinci et al., 2010). This is particularly strong at station AQK, where synthetics do not capture the low frequency amplification at about 0.6 Hz.

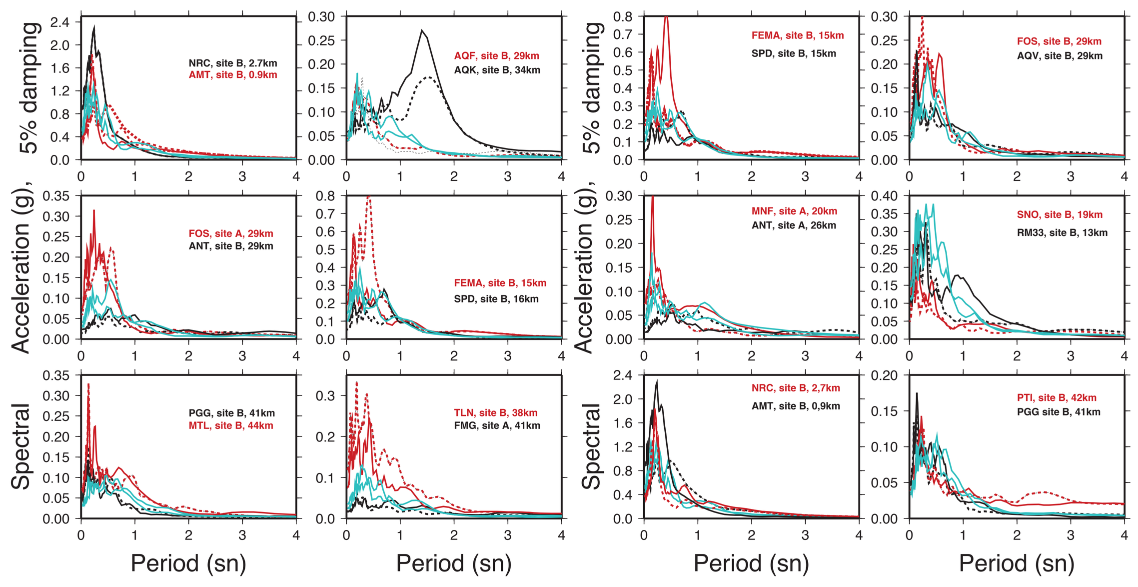

Figure 15
Acceleration response spectra at 5% damping ratio for simulated (green solid lines) and recorded (EW dashed line and NS solid line) signals. Considering similar JB distance ranges, stations in forward (red lines) and backward (black lines) directivity sectors are compared.

Conclusions

In the near field we have found that, rather than the use of GMPEs, hybrid simulations have a higher capability to detect near source effects and to reproduce the source complexity as well as the slight bilateral rupture observed by several authors (e.g., Tinti et la., 2016; Lanzano et al., 2016; Calderoni et al., 2016; Pischiutta et al., 2016). Moreover, the general good consistency found between synthetic and observed ground motion (both in the time and frequency domain), suggests that the use of regional-specific source scaling and attenuation parameters in hybrid simulations improves ground motion estimations.

Synthetic hybrid waveforms and Fourier amplitude are generally compatible with records, suggesting that our model can adequately explain amplitude levels and temporal characteristics of observed seismograms and to detect near source effects.

Finally, the use of site-specific amplification curves (at stations were the velocity profile was available) rather than the site-classes as prescribed by NTC-08 seismic code, led to a further reduction of residuals between observed and simulated.

REFERENCES : Akinci, A., Malagnini, L., Sabetta, F. (2010). Characteristics of the strong ground motions from the 6 April 2009 L'Aquila earthquake, Italy. Soil Dyn. Earthq. Eng., 30: 320–335. Bindi, D., Pacor, F., Luzi, L., Puglia, R., Massa, M., Ameri, G., Paolucci, R. (2011). Ground motion prediction equations derived from the Italian strong motion database. Bull Earthquake Eng (2011) 9:1899–1920 doi 10.1007/s10518-011-9313-z. | Boore, D.M. and Atkinson, G.M., (2008). Ground-motion prediction equations for the average horizontal component of PGA, PGV, and 5 per centdamped PSA at spectral periods between 0.01 s and 10.0 s. Earthq. Spectra, 24: 99–138. | Calderoni, G., Rovelli, R., Di Giovambattista, R. (2016). Evidence of bilateral rupture in the Mw 6.0, Amatrice earthquake of 24 August 2016. DOI:10.5281/zenodo.61713 | Cirella A., and A. Piatanesi (2016). Source Complexity of the 2016 Amatrice Earthquake from Non Linear Inversion of Strong Motion Data: Preliminary Results; DOI:10.5281/zenodo.153821 | De Luca S, Marcucci G, Milana T, Sano' (2005). Evidence of low frequency amplification in the City of L'Aquila, Central Italy, through a multidisciplinary approach including strong- and weak-motion data, ambient noise, and numerical modeling. Bull. Seismol. Soc. Am., 95:1469–81.| Dreger, D. S., L. Gee, P. Lombard, M. H. Murray, and B. Romanowicz (2005), Rapid finite-source analysis and near-fault strong ground motions:Application to the 2003 Mw 6.5 San Simeon and 2004 Mw 6.0 Parkfield earthquakes, Seismol. Res. Lett., 76(1), 40–48. | Hartzell, S. H., and T. H. Heaton (1983), Inversion of strong ground motion and teleseismic waveform data for the fault rupture history of the 1979 Imperial Valley, California, earthquake, Bull. Seismol. Soc. Am, 73(6), 1553–1583. | Herrero, A., and P. Bernard (1994). A kinematic self-similar rupture process for earthquakes, Bull. Seismol. Soc. Am. 84, no. 4, 1216–1228. | Herrmann, R. B., L. Malagnini, and I. Munafò (2011), Regional moment tensor of the 2009 L'Aquila earthquake sequence, Bull. Seismol. Soc. Am., 101(3), 975–993. | Lanzano G., Luzi L., Pacor F., Puglia R., D'Amico M., Felicetta C., Russo E. (2016). Preliminary analysis of the accelerometric recordings of the August 24th, 2016 MW 6.0 Amatrice earthquake Annals of Geophysics, 59, Fast Track 5, 2016. | Motazedian, D., and G. M. Atkinson (2005). Stochastic finite-fault modeling based on a dynamic corner frequency, Bull. Seismol. Soc. Am. 95, 995–1010, doi: 10.1785/0120030207. | Pischiutta, M., Akinci, A., Malagnini, L., Herrero, A., Characteristics of the Strong Ground Motion from the 24th August 2016 Amatrice Earthquake, Annals of Geophysics, 59, Fast Track 5, 2016. | Ruiz, J. A., D. Baumont, P. Bernard, and C. Berge-Thierry (2011). Modelling directivity of strong ground motion with a fractal, k–2 kinematic source model, Geophys. J. Int. 186, 226–244 . | Ren, Y., Wang, H., Wen, R., 2017. Imprint of Rupture Directivity From Ground Motions of the 24 August 2016 Mw6.2 Central Italy Earthquake, Tectonics, https://doi.org/10.1002/2017TC004673 | Ruiz, J. A., D. Baumont, P. Bernard, and C. Berge-Thierry (2011). Modelling directivity of strong ground motion with a fractal, k–2 kinematic source model, Geophys. sion. Geophys. Res. Lett., 43, 10,745–10,752, doi:10.1002/2016GL071263.